

1  
2  
3  
4  
5  
6  
7  
8  
9  
10  
11  
12  
13  
14  
15  
16  
17  
18

**The East Atlantic / West Russia teleconnection in the North Atlantic: climate  
impact and relation to Rossby wave propagation**

Young-Kwon Lim

NASA Goddard Space Flight Center, Global Modeling and Assimilation Office,  
Goddard Earth Sciences Technology and Research / I. M. System Group,  
Greenbelt, Maryland, 20771, U.S.A.  
Young-Kwon.Lim@nasa.gov

Submitted to Climate Dynamics  
February 08, 2014

Abstract

19  
20  
21  
22  
23  
24  
25  
26  
27  
28  
29  
30  
31  
32  
33  
34  
35  
36  
37  
38  
39  
40  
41

Large-scale winter teleconnection of the East Atlantic / West Russia (EA/WR) over the Atlantic and surrounding regions is examined in order to quantify its impacts on temperature and precipitation and identify the physical mechanisms responsible for its existence. A rotated empirical orthogonal function (REOF) analysis of the upper-tropospheric monthly height field captures successfully the EA/WR pattern and its interannual variation, with the North Atlantic Oscillation as the first mode. EA/WR's climate impact extends from eastern North America to Eurasia. The positive (negative) EA/WR produces positive (negative) temperature anomalies over the eastern US, western Europe and Russia east of Caspian Sea, with negative (positive) anomalies over eastern Canada, eastern Europe including Ural Mountains and the Middle East. These anomalies are largely explained by lower-tropospheric temperature advections. Positive (negative) precipitation anomalies are found over the mid-latitude Atlantic and central Russia around  $\sim 60^{\circ}\text{E}$ , where lower-level cyclonic (anticyclonic) circulation anomaly is dominant. The eastern Canada and the western Europe are characterized by negative (positive) precipitation anomalies.

The EA/WR is found to be closely associated with Rossby wave propagation. Wave activity fluxes show that it is strongly tied to large-scale stationary waves. Furthermore, a stationary wave model (SWM) forced with vorticity transients in the mid-latitude Atlantic ( $\sim 40^{\circ}\text{N}$ ) or diabatic heat source over the subtropical Atlantic near the Caribbean Sea produces well-organized EA/WR-like wave patterns, respectively. Sensitivity tests with the SWM indicate improvement in the simulation of the EA/WR when the mean state is modified to have a positive NAO component that enhances upper-level westerlies between  $40\text{-}60^{\circ}\text{N}$ .

## 42 1. Introduction

43 Large-scale teleconnection patterns that persist from days to months are known to play an  
44 important role in determining whether a particular season will be warm or cold, wet or dry. The  
45 teleconnection patterns, often defined in terms of the height and/or sea level pressure fields, and  
46 the corresponding atmospheric circulation fields typically cover vast geographical areas  
47 (Barnston and Livezey 1987).

48 The North Atlantic Oscillation (NAO) is one of the primary modes of atmospheric variation  
49 over the North Atlantic, impacting seasonal climates over North America and Europe (e.g.,  
50 Hurrell 1995; Donat et al. 2010; Sugimoto and Hanawa 2010). Other teleconnection patterns  
51 with an important component in the North Atlantic region are the Scandinavia (SCA) (Wallace  
52 and Gutzler 1981; Bueh and Nakamura 2007), the East-Atlantic (EA) (Washington et al. 2000;  
53 Bojariu and Reverdin 2002), and the East Atlantic / West Russia (EA/WR) (Barnston and  
54 Livezey 1987; Washington et al. 2000; Wang et al. 2011) patterns. While numerous earlier  
55 studies investigated the NAO because of its dominant large-scale influences on climate  
56 variability, impact of the other teleconnections on climate variability over the North Atlantic and  
57 generation of their patterns have yet to be addressed in more detail. Particularly, the EA/WR,  
58 which is characterized by two main large-scale anomalies located over the Caspian Sea and  
59 western Europe, has not attracted any significant and detailed investigation despite the  
60 recognition of EA/WR as one of the leading teleconnections over the North Atlantic (Barnston  
61 and Livezey 1987; Washington et al. 2000). Wang et al. (2011) and Lim and Kim (2013)  
62 suggested that understanding EA/WR is very important because not only its impact extends  
63 across the European mainland, but also the impact reaches mid-latitude East Asia as a planetary-

64 scale stationary wave pattern. The possible role of EA/WR in modulating the east Asian winter  
65 monsoon variability was analyzed by Wang et al. (2011) and Kim et al. (2013).

66       Regarding the interrelationship among the teleconnections over the Atlantic, Scherrer et al.  
67 (2006) investigated the possible relationship between the NAO and large-scale atmospheric  
68 blocking located over the Atlantic, the Scandinavian Peninsula, and mainland Europe.  
69 Specifically, the study identified that a change in the intensity of the westerlies over the central  
70 latitudes of the eastern North Atlantic and over much of Europe associated with the NAO, is at  
71 times associated with a long-lived atmospheric blocking in the vicinity of Great Britain and the  
72 Scandinavian Peninsula. Pavan et al. (2000) and Shabbar et al. (2001) addressed that atmospheric  
73 blocking over the North Atlantic seems more frequently observed during a substantial negative  
74 NAO. However, there are some indications that blocking-like persistent high-pressure systems  
75 over the European mainland are more related to the positive NAO phase (Wanner et al. 2001).  
76 Overall, it appears that there is still much to be learned about possible inter-relationships  
77 between the various modes, including the potential role of other key large-scale patterns (e.g.,  
78 ENSO) in modulating teleconnection patterns in this region.

79       Turning to the physical mechanisms responsible for these patterns of variability, there is  
80 some evidence for an important role of wave propagation forced by transient eddies. Bueh and  
81 Nakamura (2007) found that transient eddies migrating along the storm track together with  
82 incoming Rossby wave activity from the Atlantic are crucial for maintaining teleconnection  
83 pattern. Several other studies also argued that heating over the Atlantic may be responsible for  
84 producing the atmospheric teleconnection (e.g., Walter et al. 2001; Wang et al. 2011). Clearly,  
85 the relative importance of heating and weather transients, and the primary source regions for  
86 generating Rossby waves associated with the various Atlantic teleconnections needs clarification.

87 The purpose of this study is to provide a better (physically-based) understanding of the  
88 impacts of the EA/WR teleconnection on winter climate over the North Atlantic and surrounding  
89 regions, and their relation to Rossby wave propagation. This study takes advantage of the latest  
90 high-resolution ( $\sim 0.5^\circ$  latitude/longitude) reanalysis data to document the impacts of the EA/WR  
91 pattern on temperature and precipitation over the Arctic, western Russia, eastern North America,  
92 North Africa and Europe. The stationary wave model of Ting and Yu (1998) is used to examine  
93 the role of stationary Rossby waves in explaining the structure and forcing of these patterns.

94 Section 2 describes the data and stationary wave model utilized in this study. The capture of  
95 the EA/WR spatial pattern and its interannual variation over the study domain is described in  
96 Section 3. Section 3 also discusses the atmospheric circulation and other features associated  
97 with the EA/WR that acts to produce the regional climate impacts. Section 4 identifies the source  
98 regions and the propagation of large-scale stationary waves associated with the EA/WR pattern,  
99 and includes an assessment of the sensitivity of the response to the basic state tied to variations  
100 in the NAO or ENSO. This is followed by the concluding remarks in Section 5.

101

## 102 **2. Data and Model**

103 This study uses the Modern-Era Retrospective analysis for Research and Applications  
104 (MERRA) reanalysis data (Rienecker et al. 2011) to analyze the past 33 winters (December,  
105 January, February or DJF) from 1979/80 through 2011/12. The key variables consist of SST,  
106 upper-level (250hPa and 300hPa) geopotential height, wind (300hPa and 850hPa), temperature  
107 (300hPa, 850hPa, and 2 meter level), sea level pressure (SLP), diabatic heating (residually  
108 diagnosed), and precipitation. The horizontal resolution is  $0.5^\circ$  latitude  $\times$   $0.6667^\circ$  longitude, and  
109 the temporal resolution is daily though the daily values are averaged to create monthly means.

110 The stationary wave model is a fully nonlinear baroclinic model with 14 vertical levels on  
111 sigma coordinates with R30 truncation in the horizontal (Ting and Yu 1998). The model  
112 variables include vorticity, divergence, vertical velocity (sigma coordinate), surface pressure,  
113 geopotential height, and temperature. A rigid-lid boundary condition is applied at the top and the  
114 surface of the model atmosphere. For damping, Rayleigh friction and Newtonian cooling are  
115 applied in the vorticity, divergence, and temperature equations to ensure meaningful solutions.  
116 For further details of the model see Ting and Yu (1998).

117

### 118 **3. Impact of the EA/WR pattern on temperature and precipitation**

119 The leading modes of large-scale teleconnections are computed from the monthly mean  
120 upper-level (250hPa) geopotential height field. The climatologies for each month of DJF were  
121 first removed from the raw data. A rotated EOF (REOF) technique (Richman 1986) was applied  
122 to the resulting anomaly data spanning the past 33-winters. The first four REOFs, in order of  
123 decreasing variance, are the NAO (Wallace and Gutzler 1981; Barnston and Livezey 1987), the  
124 SCA (Washington et al. 2000; Bueh and Nakamura 2007), the EA (Barnston and Livezey 1987;  
125 Bojariu and Reverdin 2002), and the EA/WR (Barnston and Livezey 1987; Washington et al.  
126 2000). Please note that a previous study using an alternative rotation method also captured the  
127 NAO as the first mode followed by SCA (Hannachi et al. 2009). The eigenvectors (the spatial  
128 distributions) are shown in the left panel of Figure 1, with the corresponding principal  
129 component (PC) time series shown in the right panel. Note that all spatial patterns and PC time  
130 series are plotted for what is conventionally considered to be the positive phase of the pattern.  
131 Also shown in the right panel are the teleconnection indices archived at the National Oceanic and  
132 Atmospheric Administration (NOAA)/National Center for Environmental Prediction

133 (NCEP)/Climate Prediction Center (CPC) (<ftp://ftp.cpc.ncep.noaa.gov/wd52dg/>  
134 [data/indices/tele\\_index.nh](ftp://ftp.cpc.ncep.noaa.gov/wd52dg/data/indices/tele_index.nh)). The PC time series and the index time series are in good agreement,  
135 confirming that the previously identified teleconnection patterns have been successfully captured.  
136 This study has examined the sensitivity of the patterns to the domain size (e.g., to include the  
137 entire northern hemisphere) and found that the spatial distributions of the REOFs are robust with  
138 respect to changes in the domain (figure not shown). Note that an AO (Thompson and Wallace,  
139 1998) mode was captured as the fourth REOF (not shown), though in our regional analysis, the  
140 NAO likely already includes some of the variability of the AO.

141 The EA/WR pattern (REOF 4), the main focus of the present study, has two large-scale  
142 anomaly centers located just north of the Caspian Sea and western Europe, influencing Eurasian  
143 climates (Figure 1d). During the positive phase of the EA/WR, a negative height anomaly  
144 occurs over the Atlantic near 40°W and 40-45°N, while a positive anomaly is found over central  
145 Europe (0-30°E). The EA/WR appears to originate in the North Atlantic and extends  
146 northeastward across Europe and European Russia (Barnston and Livezey 1987; Washington et  
147 al. 2000).

148 In order to quantify the temperature and precipitation anomalies associated with each  
149 teleconnection pattern, and to help explain how those anomalies are produced in different regions,  
150 several atmospheric variables at low levels (i.e., near surface and 850hPa) are regressed onto the  
151 time series associated with each z250 hPa height PC. In particular, the regressed field ( $R_M(x, y)$ )  
152 for the Mth mode at grid point (x,y) is defined as

$$153 \quad R_M(x, y) = \sum_{t=1}^{nt} T(x, y, t) \cdot P_M(t), \quad (1)$$

154 where  $T(x, y, t)$  is the anomaly field in question at time step t, and  $P_M(t)$  represents the

155 normalized monthly PC time series of the z250 hPa height for the Mth mode. In the above  
156 summation,  $nt$  is equal to 99 months, the length of the analysis period.

157 In this study, the advective temperature change arising from the circulation anomaly is  
158 calculated as  $-V_{T_{sl}} \cdot \nabla T_{Cli}$  (Linkin and Nigam 2008), where  $V_{T_{sl}}$  indicates the horizontal winds  
159 associated with the EA/WR pattern and  $T_{Cli}$  refers to the climatological temperatures (Figure 2c).  
160 Note that the contribution from the nonlinear component,  $-V_{T_{sl}} \cdot \nabla T_{T_{sl}}$ , and the other linear  
161 component,  $-V_{Cli} \cdot \nabla T_{T_{sl}}$ , is by comparison small.

162 In general, the geographical distribution of the variables in Figure 2 reflects the upper-level  
163 height anomaly distribution that has a wave structure spanning the Atlantic, Europe, and western  
164 Russia shown in Figure 1 (cf., Barnston and Livezey 1987; Washington et al. 2000). Such a wave  
165 structure is expected to be associated with circulation anomalies and temperature advection  
166 patterns that produce regions of alternating warm and cold weather. Figure 2b clearly shows a  
167 strong anticyclonic circulation over Europe and cyclonic circulation over western Russia in the  
168 event of positive EA/WR. These anomaly pattern helps to determine temperature advection  
169 characterized by warm advection over the northeast Atlantic extending into western Europe and  
170 western Africa ( $\sim 20^{\circ}W \sim 10^{\circ}E$ ), and Russia northeast of the Caspian Sea. Cold advection occurs  
171 primarily over eastern Canada, and Russia near the Ural Mountains (Figure 2c), where northerly  
172 flow located west of the negative SLP anomaly is dominated.

173 The resulting temperature anomaly pattern in Figure 2a reflects this spatial distribution of  
174 circulation and temperature advection with the strongest response occurring over Russia. Figure  
175 2a reveals that the 2-meter air temperature (T2m) anomalies associated with the EA/WR extend  
176 to North America, the Middle East, Africa, and Eurasia. Western Russia shows larger magnitude  
177 of T2m anomalies ( $>1^{\circ}C$ ) than the magnitude of anomalies over the other regions (Figure 2a).



178 During the positive EA/WR, positive anomalies are found over the eastern US, western Europe,  
179 and Russia east of Caspian Sea. Eastern Canada, far eastern Europe including Ural Mountains  
180 ( $\sim 60^\circ\text{E}$ ), the Middle East and northeastern Africa regions are characterized by negative  
181 anomalies, although the anomalies are not statistically significant at the 10% level over part of  
182 the regions.

183 Figure 2d shows that distribution of precipitation anomalies is strongly coupled with the  
184 anomalous SLP and lower-level circulation pattern (Figure 2b). The positive precipitation  
185 anomalies are clearly found where negative SLP anomalies are located, and the opposite is true  
186 for the negative precipitation anomalies. During the positive EA/WR, the mid-latitude Atlantic  
187 and the central Russia ( $\sim 60^\circ\text{N}$ ) are the main regions that have the above-average precipitation,  
188 while the eastern Canada and European region experience the below-average precipitation. A  
189 weak positive precipitation anomaly is observed over the eastern US, but the magnitude is  
190 relatively small. The anomalies described in Figure 2 are of course by definition of opposite sign  
191 for the negative phase of the EA/WR.

192

#### 193 **4. The Connection with Rossby Waves**

##### 194 *a. Wave activity fluxes*

195 In this section the relationship between the EA/WR teleconnection pattern and large-scale  
196 Rossby waves is examined. Wave activity flux (WAF) vectors are calculated to identify the  
197 spatial distribution of wave propagation associated with the EA/WR. Following Plumb (1985),  
198 the stationary WAF is given as

$$F_s = p \cos \varphi \left( \begin{array}{c} v'^2 - \frac{1}{2\omega \sin \varphi} \frac{\partial(v' \Phi')}{\partial \lambda} \\ -u'v' + \frac{1}{2\omega a \sin 2\varphi} \frac{\partial(u' \Phi')}{\partial \lambda} \\ \frac{2\omega \sin \varphi}{S} \left[ v'T' - \frac{1}{2\omega a \sin 2\varphi} \frac{\partial(T' \Phi')}{\partial \lambda} \right] \end{array} \right)$$

199

200

201

202

203

204

205

206

where the variables  $(u, v)$ ,  $p$ ,  $T$ , and  $\Phi$  represent the zonal and meridional wind, pressure, temperature, and geopotential height, respectively, and where  $\lambda$  and  $\varphi$  represent longitude and latitude. The constant  $\omega$  is the earth's rotation rate ( $=7.292 \times 10^{-5}$  rad  $s^{-1}$ ) and  $a$  is the radius of the earth. The prime denotes the deviation from the zonal mean at each latitude and height.  $S = \frac{\partial \hat{T}}{\partial z} + \frac{\kappa \hat{T}}{H}$  is the static stability; the caret indicates an areal average over the Northern Hemisphere;  $\kappa$  ( $=287$  J  $K^{-1}$   $kg^{-1}/1004$  J  $K^{-1}$   $kg^{-1}$ ) is the ratio of gas constant to specific heat at constant pressure, and  $H$  is a constant scale height.

207

208

209

210

211

Figure 3 shows the horizontal WAF distribution at 300hPa. The pattern suggests that the EA/WR reflects Rossby waves responding to forcing in the mid-latitude Atlantic. Specifically, there is a clear wave train extending across the Atlantic, western Europe and Russia associated with the EA/WR.

212

### *b. Rossby wave source*

213

214

215

216

217

218

The source regions and the propagation characteristics of the EA/WR teleconnection are investigated in this section using the stationary wave model (SWM) of Ting and Yu (1998) (see section 2 for the model description). This study focuses on both diabatic heat forcing and transient vorticity forcing, the importance of which in generating large-scale wave trains in the extratropics has been shown by previous studies (Sardeshmukh and Hoskins 1988; Qin and Robinson 1993). Also, the upper-level WAF pattern (Figure 3) suggests that the Rossby wave

219 source (RWS) is located over the extratropical Atlantic, in a region where transient eddies  
220 associated with the Atlantic storm track could play a role (Bueh and Nakamura 2007). Previous  
221 studies emphasize the importance of changes in wintertime extratropical transient eddy activity  
222 for forcing changes in upper-level jet intensity and its extension (e.g., Losada et al. 2007).

223 Following Schubert et al. (2011) this study attempts to reproduce the observed  
224 teleconnection patterns by forcing the SWM model with a series of regional heat and vorticity  
225 forcing functions, respectively, located at  $5^\circ$  longitude/latitude intervals distributed throughout  
226 the North Atlantic. The 3-dimensional basic state for this run is the MERRA climatology  
227 computed from the past 33 winters (1979/80-2011/12). The similarity is assessed between the  
228 SWM response to each forcing function and the observed teleconnection by calculating their  
229 spatial correlation over the North Atlantic and Europe domain ( $60^\circ\text{W}$ - $60^\circ\text{E}$ ,  $20$ - $80^\circ\text{N}$ ). These  
230 correlations are then plotted at the forcing locations (Figure 4).

231 Figure 4a shows that the largest correlations for the SWM response to heat forcing are found  
232 over the subtropical western Atlantic near the Caribbean Sea. Correlation values over the mid-  
233 latitude Atlantic are generally small. The subtropical region where the largest correlation is  
234 found is consistent with the region of the largest positive diabatic heating anomaly (Figure 4b) at  
235 mid-troposphere and SST anomaly (Figure 4c) regressed onto the EA/WR, indicating a possible  
236 heat source over the region to generate the Rossby-type wave that resembles the EA/WR. This  
237 possible positive relationship between SST anomaly over the subtropical western Atlantic and  
238 the phase of EA/WR is in good agreement with Wang et al. (2011). The study suggested that  
239 cold North Atlantic SST anomalies are associated with the negative EA/WR pattern that  
240 enhances the Siberian high and east Asian winter monsoon.

241 As for the transient vorticity forcing, Figure 5a shows that the EA/WR has spatial  
242 correlations greater than 0.7 over the mid-latitude Atlantic basin ( $\sim 40^\circ\text{W}$ ,  $\sim 40^\circ\text{N}$ ), suggesting  
243 they have a substantial Rossby wave component that resembles the EA/WR pattern driven by  
244 extratropical transients. It also suggests that this wave pattern is most easily forced in the central  
245 North Atlantic near the climatological jet exit region (please see the superimposed contours in  
246 Figure 5a). Blackburn and Hoskins (2001) found that the exit region of the Atlantic jet stream  
247 was important for cyclone growth and dynamically forced ascent. Distribution of upper-level  
248 (250hPa) daily zonal wind variance in Figure 5b shows the largest variance over this mid-latitude  
249 North Atlantic, indicating the strongest transient eddy activity around the wave source region.

250 Figure 6 shows some examples of the SWM response to idealized forcing chosen to  
251 resemble the observed EA/WR. The location of the heat forcing and vorticity forcing,  
252 respectively, was chosen based on the location of the largest correlation values in Figures 4 and 5  
253 which is  $80\text{-}70^\circ\text{W}$ ,  $20\text{-}25^\circ\text{N}$  for the heat forcing, and  $45\text{-}35^\circ\text{W}$ ,  $35\text{-}40^\circ\text{N}$  for the vorticity forcing  
254 (Figures 6a,b). The SWM responses (upper-panels) and the observed patterns captured by  
255 REOFs (lower-panels) show substantial similarities. In particular, positive heat forcing in the  
256 subtropical North Atlantic ( $20\text{-}25^\circ\text{N}$ ) and vorticity forcing in the mid-latitude Atlantic ( $35\text{-}40^\circ\text{N}$ ),  
257 respectively, generates a stationary wave with maximum amplitude over the high latitude North  
258 Atlantic, the Scandinavian peninsula, and the Eurasian continent (Figures 6a,b), similar to the  
259 observed EA/WR pattern in Figure 6c. The SWM, however, also generates a low latitude  
260 response (Figure 6a) that is not found in the observed pattern. Overall, Figure 6 supports the idea  
261 that EA/WR pattern is associated with large-scale Rossby wave responses to diabatic heat  
262 forcing and vorticity forcing over the extratropical Atlantic.

263 Next, rather than deducing the RWS based on the SWM responses to idealized forcing, the  
 264 RWS is estimated directly based on observation data (MERRA data). Following Sardeshmukh  
 265 and Hoskins (1988) and Qin and Robinson (1993), the RWS is derived from the quasi-  
 266 geostrophic vorticity equation as

$$267 \quad \text{RWS} = -\mathbf{V}_x \cdot \nabla(\zeta + f) - (\zeta + f)\nabla \cdot \mathbf{V}_x \quad (1)$$

268 where  $\mathbf{V}_x$  is the divergent (irrotational) wind vector,  $\zeta$  the relative vorticity, and  $f$  the Coriolis  
 269 parameter. The linearized form of RWS can be written as

$$270 \quad \text{RWS}_L = -\mathbf{V}'_x \cdot \nabla(\bar{\zeta} + f) - (\bar{\zeta} + f)\nabla \cdot \mathbf{V}'_x - \zeta' \nabla \cdot \bar{\mathbf{V}}_x - \bar{\mathbf{V}}_x \cdot \nabla \zeta', \quad (2)$$

271 where the overbar denotes the climatological mean and the prime denotes the anomaly associated  
 272 with the teleconnection pattern (e.g., EA/WR). The first and fourth term on the right hand side  
 273 of (2) are associated with vorticity advection, whereas the second and third terms involve the  
 274 generation of wave vorticity by the divergence of the divergent wind (i.e., vorticity stretching).  
 275 Sardeshmukh and Hoskins (1988) and Qin and Robinson (1993) found that the first and fourth  
 276 terms capture the main features of the tropical source whereas the second and third terms  
 277 determine the main features of the extratropical RWS (Seo and Son 2012). Figure 7a shows the  
 278 distribution of the RWSs characterized by positive peak over the mid-latitude Atlantic. Location  
 279 of the peak values at 50-30°W and 35-50°N is consistent with the positive spatial correlation  
 280 maximum shown in Figure 5a.

281 In order to confirm that the regions forcing the EA/WR wave patterns are indeed in the  
 282 locations we discussed in Figures 4 through 6, the EA/WR pattern is reproduced with the RWS  
 283 forcing in the region outlined in Figures 7a. The region is upstream of the EA/WR pattern, and  
 284 located where the magnitude of spatial correlation between the patterns of observed  
 285 teleconnection and idealized model result (by transient vorticity forcing) is high (Figure 5a). The

286 responses to the forcing in those regions (Figure 7b) show a reasonable similarity with the  
287 observed EA/WR pattern captured by the REOFs (Figure 6c).

288

289 *c. Sensitivity to background flow change (NAO and ENSO)*

290 Since variations in the NAO impact the upper-level westerlies over the North Atlantic, this  
291 study examines whether the NAO has an impact on the other patterns through NAO-related  
292 changes in the base state. Table 1 shows the variance of the PCs of the EA/WR REOFs for  
293 different NAO phases. The results show that the variances of the PCs are larger on average in  
294 the event of a positive NAO. The dependency of the intensity of the EA/WR pattern upon the  
295 NAO phase indicates that strong wind and storminess over the European mainland is more likely  
296 to occur during the positive NAO, as suggested by Donat et al. (2010).

297 In order to more clearly demonstrate that the EA/WR pattern is indeed sensitive to the NAO  
298 phase, the SWM response to vorticity sources is re-examined with modified base states. In  
299 particular, this examination considers base states that have added to it +/- one standard deviation  
300 of the NAO pattern. Additional experiments were conducted by incorporating +/- one standard  
301 deviation of the ENSO component<sup>1</sup>. Figure 8 shows the changes made to the base state, with one  
302 standard deviation of the positive (negative) NAO (Fig. 8a) acting to accelerate (decelerate) the  
303 westerlies between 40-60°N over the Atlantic, and decelerate (accelerate) them between 20-40°N.  
304 El Niño also plays a role in displacing the Atlantic storm track and modifying the westerlies, but  
305 with smaller magnitude compared with the NAO impact (Figure 8b).

306 Four SWM experiments were conducted to quantify the impact of the NAO and ENSO on  
307 the EA/WR. Figure 9 shows the EA/WR response to the positive NAO (Figure 9a) and negative

---

<sup>1</sup> Note that the ENSO component is captured as a higher REOF (not shown) occurring just after the EA/WR mode.

308 NAO (Figure 9b), respectively. The transient vorticity forcing is identical to that referred to in  
309 Figure 5. An EA/WR-like pattern is generated for both basic states (Figures 9a,b), though there  
310 are differences in the intensities of the ridges/troughs between the two wave patterns. The wave  
311 path is also different. In general, EA/WR is better organized and strengthened over the Atlantic  
312 and western Europe when the mean state is modified with a positive NAO component. This is, to  
313 a great extent, consistent with Wanner et al. (2001) and Scherrer et al. (2006) who found a  
314 greater possibility of strong pressure patterns (teleconnection) and atmospheric blocking over the  
315 European mainland during the positive phase of the NAO. The wave track is also more realistic  
316 with the positive NAO added to the base state (Figure 9a). For the case of the negative NAO,  
317 there is a northward displacement of the anomalies making the response less like the observed  
318 EA/WR pattern (Figure 9b). Also, the pattern shows relatively smaller amplitude especially over  
319 the Atlantic and western Europe. It appears that the stronger upper-level westerly jet at 40-60°N  
320 over the Atlantic during the positive NAO may facilitate the eastward propagation of the EA/WR  
321 over the European continent. In contrast, the main anomalies during the negative NAO tend to be  
322 situated further west over Greenland due to weakened upper-level westerlies between 40-60°N.

323 The above experiments were repeated for the modified mean states reflecting the ENSO  
324 impact. The results show some differences in the EA/WR pattern for the El Niño and La Niña  
325 cases, but the differences are considerably less than those for the NAO shown in Figure 9,  
326 reflecting the smaller change in the upper-level jet compared to that associated with the NAO  
327 (figure not shown). This suggests that a very strong ENSO is necessary to noticeably modulate  
328 the EA/WR patterns, and that in general the NAO is a greater factor in modulating those patterns.

329

## 330 **5. Concluding remarks**

331 This study has investigated the EA/WR, the important winter atmospheric teleconnection  
332 pattern generated over the North Atlantic region. The focus is on providing further insights into  
333 the spatial scope and physical mechanisms of the impacts, as well as the dynamical mechanisms  
334 responsible for the existence of EA/WR.

335 It was found that the four leading REOFs of the upper tropospheric height field consist of, in  
336 order of decreasing variance, the NAO, the SCA, the EA, and the EA/WR. There have been few  
337 studies that have examined in any detail the impact of the EA/WR on regional temperatures and  
338 precipitation across Eurasia. Here the present study found that the positive (negative) EA/WR is  
339 associated with a strong warming (cooling) over Russia east of the Caspian Sea whereas it is  
340 associated with cooling (warming) over the Ural Mountains of northern Russia. The strong  
341 temperature response over those regions is linked to a surface pressure anomaly near the Ural  
342 Mountains and associated strong atmospheric circulation and thermal advection anomalies. Other  
343 impacts linked to the positive (negative) phase of the EA/WR are a warming (cooling) over the  
344 eastern US and western Europe, and a cooling (warming) over eastern Canada, far eastern  
345 Europe and the Middle East, though these tend to be weak. It was also found in this study that  
346 precipitation anomalies are strongly coupled with the anomalous SLP and lower-level circulation  
347 pattern. Positive (negative) precipitation anomalies are pronounced over the mid-latitude Atlantic  
348 and the central Russia ( $\sim 60^\circ\text{N}$ ), while the negative (positive) anomalies are mainly distributed  
349 over the eastern Canada and European region during the positive (negative) EA/WR. The eastern  
350 US region exhibits the positive (negative) anomalies, but the magnitudes are generally small  
351 during the positive (negative) phase of the EA/WR.

352 The second part of this study examined the relationship of the EA/WR teleconnection to  
353 large-scale Rossby waves. It was found, using a SWM, that the EA/WR pattern could be



354 reproduced by forcing the model with vorticity transients over the mid-latitude North Atlantic  
355 (35-40°N) and with diabatic heating over the subtropical western Atlantic (15-20°N). The results  
356 appear consistent with Bueh and Nakamura (2007) in that the transient eddies migrating along  
357 the Atlantic storm track play an important role for emanation of the Rossby waves from the mid-  
358 latitude Atlantic. The RWS calculation based on observation provides supporting evidence that  
359 the RWS regions over the Atlantic are at ~40°W and ~40°N for the EA/WR. It was further  
360 shown that it is the vorticity transients near the Atlantic jet region (~40°N, ~40°W) that are  
361 important for generating the EA/WR-like response.

362 This study found that the EA/WR-like Rossby wave responses in the SWM show some  
363 sensitivity to the base state, with better-organized eastward propagation and enhanced  
364 ridge/trough anomalies over the North Atlantic and far western Europe occurring when the base  
365 state includes a positive NAO component. This appears to be due to the enhancement of the  
366 upper-level westerlies (40-60°N) associated with the positive NAO. Less organized EA/WR  
367 pattern is simulated when the base state includes a negative NAO component. This finding  
368 appears to support the argument by earlier studies (Pavan et al. 2000; Wanner et al. 2001;  
369 Scherrer et al. 2006) that addressed weaker pressure patterns and associated blocking over the  
370 European continent during the negative NAO.

371 The modulation of the EA/WR pattern by other key large-scale modes of variability such as  
372 ENSO was also examined. The modulation of the teleconnection patterns by ENSO (El Niño  
373 versus La Niña) is less pronounced compared with the NAO impact, suggesting a greater role of  
374 NAO in modulating those teleconnection patterns. The result emphasizes the importance of  
375 upper-level westerly wind changes over the North Atlantic in modulating these teleconnection

376 patterns, suggesting that the variability in these regions consists of a complex interplay of the  
377 leading patterns.

378       This study provides fundamental assessment of the EA/WR pattern in terms of 1) its climate  
379 impact on surface temperature and precipitation over vast area across North America, North  
380 Africa and Europe including western Russia, and 2) relation of the EA/WR to Rossby wave  
381 propagation. Investigation of the EA/WR should further be complemented by more detailed  
382 studies, including predictability of the generation of EA/WR pattern. Better identification of  
383 extra-tropical heating (or cooling) over the western subtropical Atlantic and upper-level transient  
384 eddy activity near the mid-latitude central Atlantic should be a key factor for reliable prediction  
385 of the EA/WR pattern.

386

387 References

- 388 Barnston AG, Livezey RE (1987) Classification, seasonality and persistence of low-frequency  
389 atmospheric circulation pattern. *Mon Weather Rev* 115: 1083-1126
- 390 Blackburn M, Hoskins BJ (2001) The UK record-breaking wet autumn 2000. pp. 38–40 in UK  
391 Universities Global Atmospheric Modelling Programme, UGAMP Newsletter 24. Available  
392 from Meteorological Department, University of Reading, UK.
- 393 Bojariu R, Reverdin G (2002) Large-scale variability modes of freshwater flux and precipitation  
394 over the Atlantic. *Clim Dyn* 18: 369-381 DOI:10.1007/s003820100182
- 395 Bueh C, Nakamura H (2007) Scandinavian pattern and its climate impact. *Quart J Royal Meteor*  
396 *Sci* 133: 2117-2131
- 397 Donat MG, Leckebusch GC, Pinto JG, Ulbrich U (2010) Examination of wind storms over  
398 Central Europe with respect to circulation weather types and NAO phases. *Int J Climatol*  
399 30: 1289-1300
- 400 Hannachi A, Unkel S, Trendafilov NT, Jolliffe IT (2009) Independent component analysis of  
401 climate data: A new look at EOF rotation. *J Clim* 22: 2797-2812
- 402 Hurrell JW (1995) Decadal trends in the North Atlantic Oscillation: Regional temperatures and  
403 precipitation. *Science* 269: 676-679
- 404 Kim YJ, Kim KY, Jhun JG (2013) Seasonal evolution mechanism of the East Asian winter  
405 monsoon and its interannual variability. *Clim Dyn* 41: 1213-1228
- 406 Lim YK, Kim HD (2013) Impact of the dominant large-scale teleconnections on winter  
407 temperature variability over East Asia. *J Geophys Res* 118: 7835-7848  
408 doi:10.1002/jgrd.50462

409 Linkin ME, Nigam S (2008) The North Pacific Oscillation-West Pacific teleconnection pattern:  
410 Mature-phase structure and winter impacts. *J Clim* 21: 1979-1997

411 Losada T, Rodriguez-Fonseca B, Mechoso CR, Ma HY (2007) Impact of SST anomalies on the  
412 North Atlantic atmospheric circulation: a case study for the northern winter 1995/1996.  
413 *Clim Dyn* 29: 807-819

414 Pavan V, Tibaldi S, Brankovic C (2000) Seasonal prediction of blocking frequency: Results from  
415 winter ensemble experiments. *Quart J Roy Meteor Soc* 126: 2125-2142

416 Plumb RA (1985) On the three-dimensional propagation of stationary waves. *J Atmos Sci* 42:  
417 217-229

418 Qin J, Robinson WA (1993) On the Rossby wave source and the steady linear response to  
419 tropical forcing. *J Atmos Sci* 50: 1819-1823

420 Richman MB (1986) Rotation of principal components. *J Climatol* 6: 293–335

421 Rienecker MM, et al. (2011) MERRA – NASA’s Modern-Era Retrospective Analysis for  
422 Research Applications. *J Clim* 24: 3624-3648

423 Sardeshmukh PD, Hoskins BJ (1988) The generation of global rotational flow by steady  
424 idealized tropical divergence. *J Atmos Sci* 45: 1228-1251

425 Shabbar A, Huang J, Higuchi K (2001) The relationship between the wintertime North Atlantic  
426 Oscillation and blocking episodes in the North Atlantic. *Int J Climatol* 21: 355-369

427 Scherrer SC, Croci-Maspoli M, Schwierz C, Appenzeller C (2006) Two-dimensional indices of  
428 atmospheric blocking and their statistical relationship with winter climate patterns in the  
429 Euro-Atlantic region. *Int J Climatol* 26: 233-249

430 Schubert SD, Wang H, Suarez M (2011) Warm season subseasonal variability and climate  
431 extremes in the Northern hemisphere: The role of stationary Rossby waves. *J Clim* 24:  
432 4773-4792

433 Seo KH, Son SW (2012) The global atmospheric circulation response to tropical diabatic heating  
434 associated with the Madden-Julian Oscillation during northern winter. *J Atmos Sci* 69:  
435 79-96

436 Sugimoto S, Hanawa K (2010) The wintertime wind stress curl field in the North Atlantic and its  
437 relation to atmospheric teleconnection patterns. *J Atmos Sci* 67: 1687-1694

438 Thompson DWJ, Wallace JM (1998) The Arctic oscillation signature in the wintertime  
439 geopotential height and temperature fields. *Geophys Res Lett* 25(9): 1297-1300  
440 doi:10.1029/98GL00950

441 Ting M, Yu L (1998) Steady response to tropical heating in wavy linear and nonlinear baroclinic  
442 models. *J Atmos Sci* 55: 3565-3582

443 Walter K, Luksch U, Fraedrich K (2001) A response climatology of idealized midlatitude  
444 thermal forcing experiments with and without a storm track. *J. Clim* 14: 467–484.

445 Wallace JM, Gutzler DS (1981) Teleconnections in the geopotential height field during the  
446 Northern Hemisphere winter. *Mon Weather Rev* 109: 784–812

447 Wang X, Wang C, Zhou W, Wang D, Song J (2011) Teleconnected influence of North Atlantic  
448 sea surface temperature on the El Niño onset. *Clim Dyn* 37: 663-676  
449 DOI:10.1007/s00382-010-0833-z

450 Wanner H, Brönnimann S, Casty C, Gyalistras D, Luterbacher J, Schmutz C, Stephenson DB,  
451 Xoplaki E (2001) North Atlantic Oscillation – concepts and studies. *Surveys in Geophys*  
452 22: 321-382

453 Washington R, Hodson A, Isaksson E, Macdonald O (2000) Northern hemisphere teleconnection  
454 indices and the mass balance of Svalbard glaciers. *Int J Climatol* 20: 473-487

455 Table 1 Variance of the principal components for EA/WR with respect to the phase of  
456 NAO. Numeric range in each cell represents the 90% confidence interval .

	EA/WR
NAO (+) (17 yrs)	1.28 0.57~2.00
NAO (-) (15 yrs)	0.72 0.30~1.14

457

458

459

REOFs of the DJF Z250 (1979DEC-2012FEB)

460

461

462

463

464

465

466

467

468

469

470

471

472

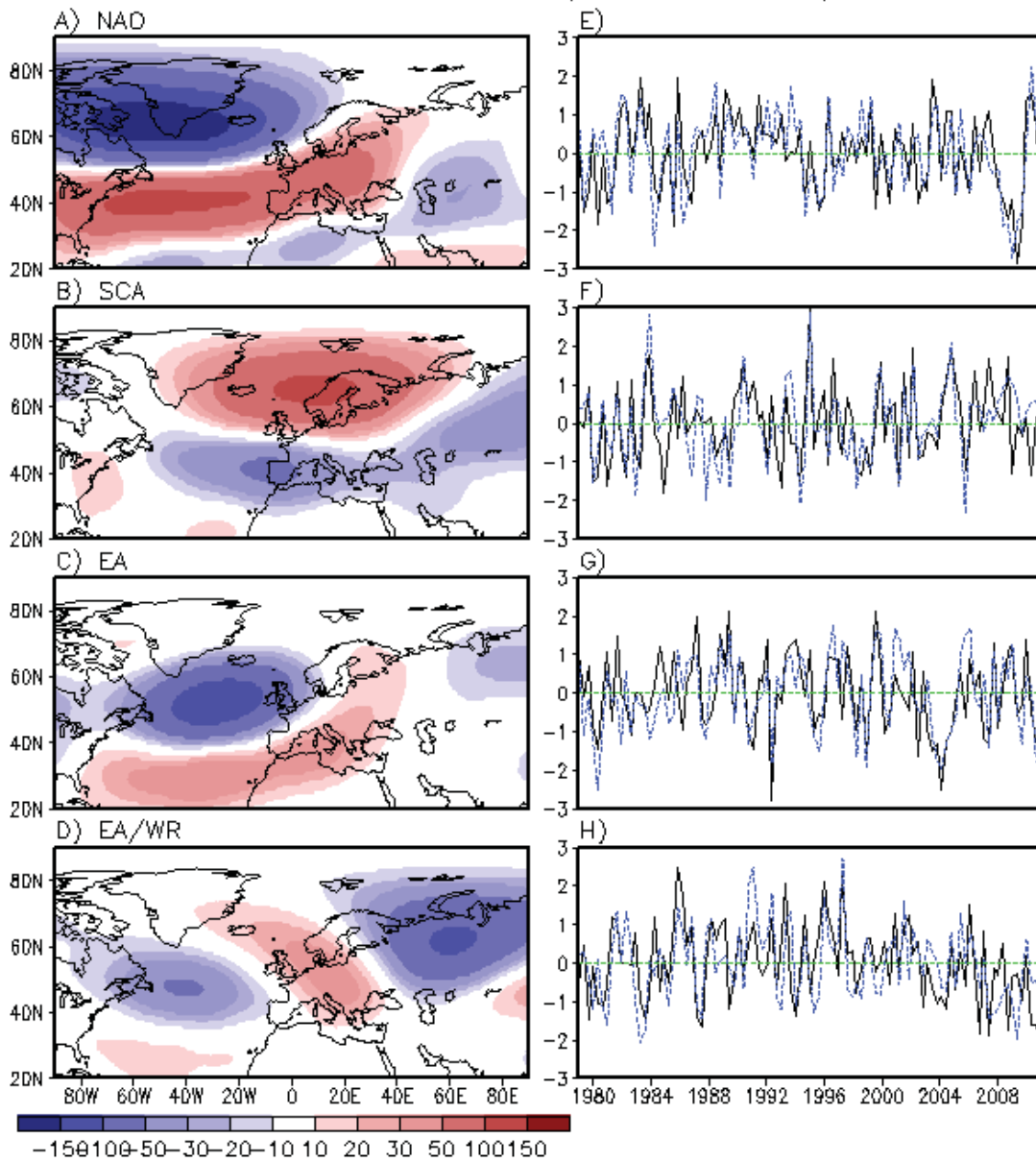
473

474

475

476

477



478 **Figure 1.** The first four rotated empirical orthogonal functions (REOFs) of the monthly 250hPa  
479 height archived from MERRA reanalysis. The data set consists of data for 33 winters from  
480 1979/80 DJF through 2011/12 DJF. The left panel represents the distribution of non-normalized  
481 eigenvectors whereas the right panel the corresponding PC represents the time series (solid line).  
482 Dashed lines denote the teleconnection pattern indices time series archived at  
483 NOAA/NCEP/CPC.



484  
 485  
 486  
 487  
 488  
 489  
 490  
 491  
 492  
 493  
 494  
 495  
 496  
 497  
 498  
 499  
 500  
 501  
 502  
 503  
 504  
 505  
 506  
 507  
 508  
 509  
 510  
 511  
 512  
 513  
 514

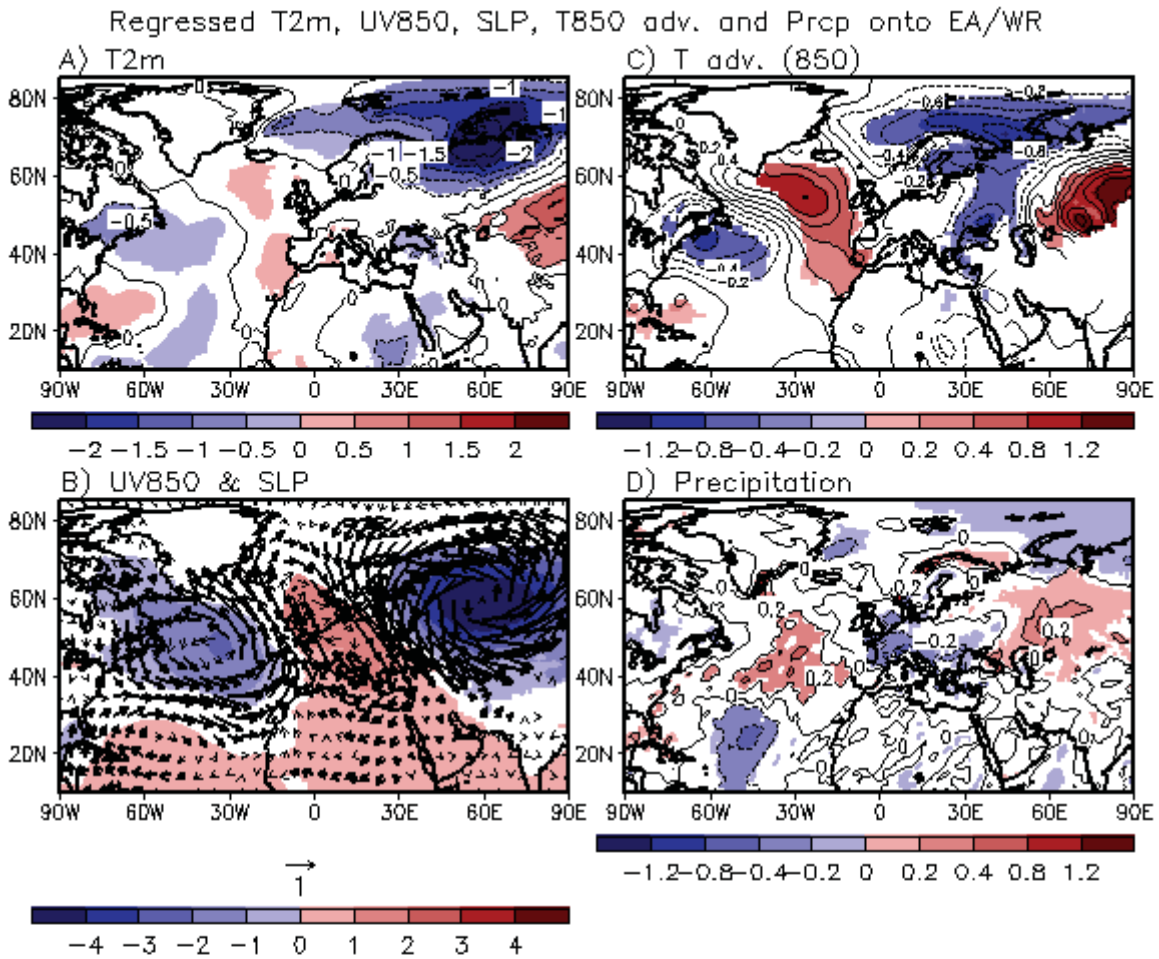


**Figure 2.** Distribution of a) 2 meter air temperature anomalies, b) sea level pressure and 850hPa circulation, c) the advective temperature change ( $-V_{Tel} \cdot \nabla T_{Cli}$ ) by 850hPa atmospheric circulation, and d) precipitation associated with 1 standard deviation in the positive EA/WR PC based on a linear regression. For the calculation of temperature advection,  $V_{Tel}$  denotes the horizontal winds regressed onto EA/WR and  $T_{Cli}$  represents the climatological temperatures. Shaded are the regions where the anomaly values are statistically significant at 10%. Wind vectors statistically significant at 10% level are plotted thick.

515  
516  
517  
518  
519  
520  
521  
522  
523  
524  
525  
526  
527  
528  
529  
530  
531  
532

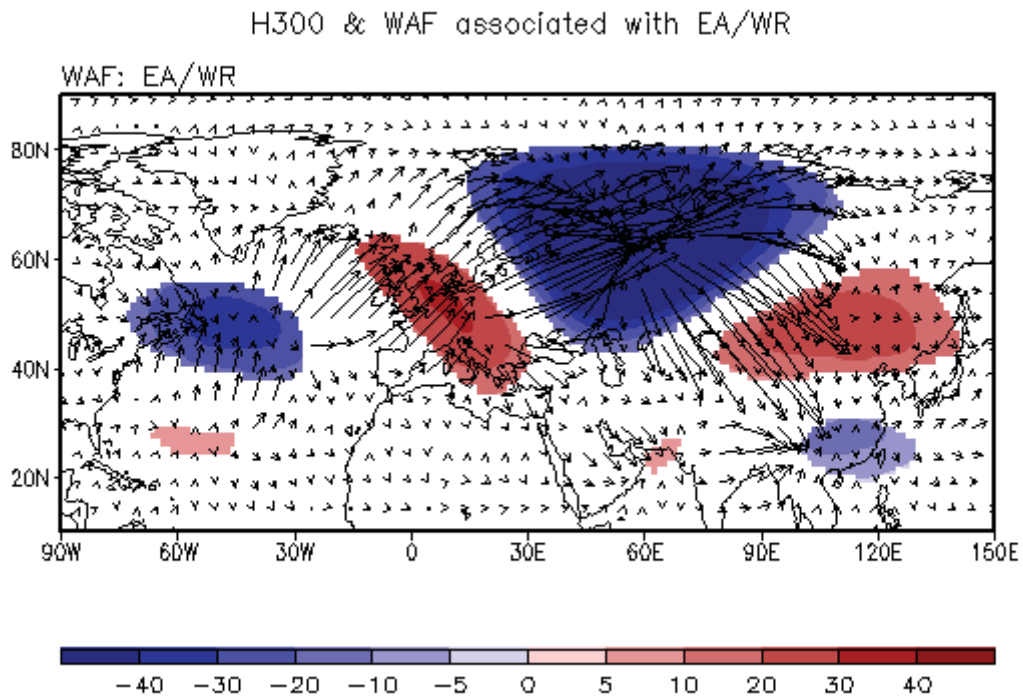


**Figure 3.** Distribution of the wave activity fluxes and geopotential height anomalies at 300hPa associated with the positive phase of EA/WR. Geopotential height anomalies statistically significant at 10% level are shaded.

533  
534  
535  
536  
537  
538  
539  
540  
541  
542  
543  
544  
545  
546  
547  
548  
549  
550  
551  
552  
553  
554  
555  
556  
557  
558  
559  
560  
561

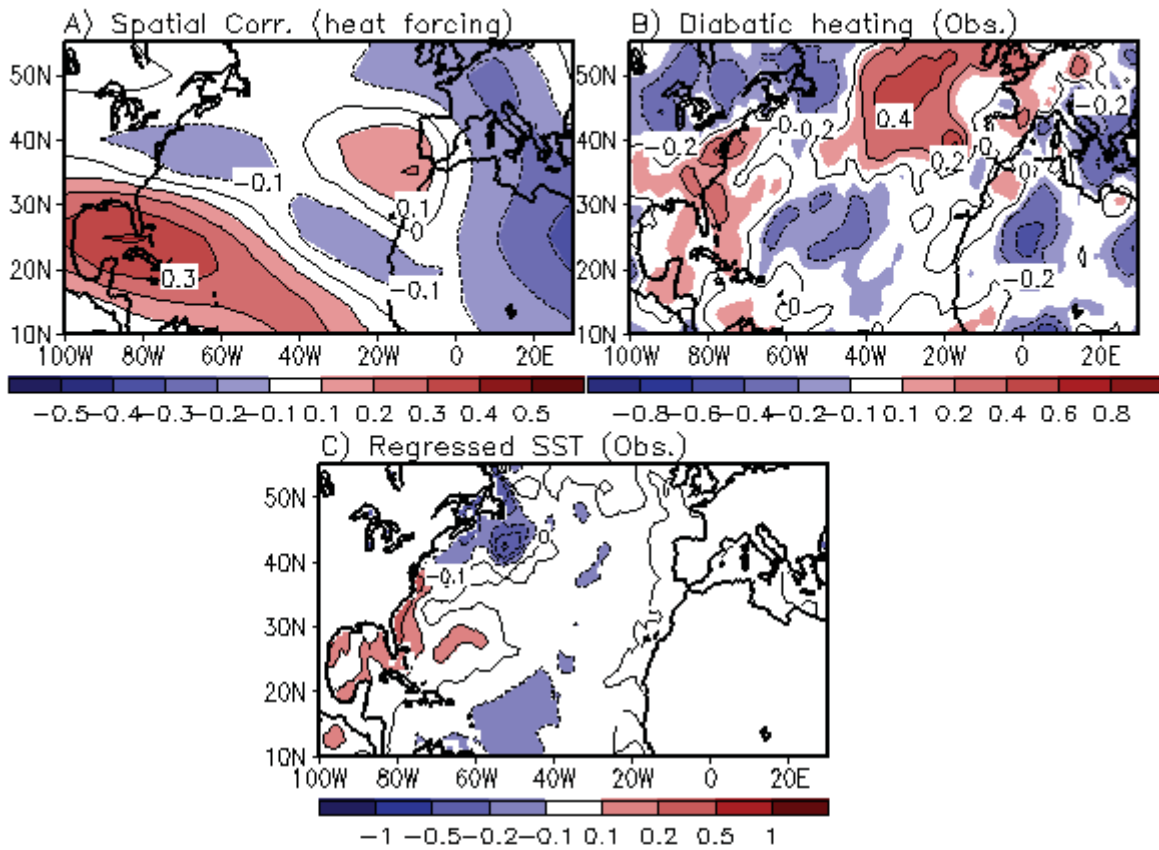


**Figure 4.** a) Spatial correlations between the observational teleconnection pattern captured by REOF and stationary wave propagation pattern produced by the stationary wave model. The 3-dimensional basic state in the SWM is the MERRA climatology computed from the past 33 winters (1979/80-2011/12). In order to generate the stationary wave at each grid point, diabatic heat forcings with the maximum at mid-troposphere are given, respectively, at the grid points with 5-degree longitude-latitude interval over the Atlantic. Geographical domain for spatial correlation calculation is 60°W~60°E and 20°N~80°N. Correlation values are plotted on the grid points where the diabatic heat forcing is given for generating the stationary wave in the model. b) represents the observed distribution of residually diagnosed diabatic heating anomalies at mid-troposphere (700-300hPa) regressed onto the EA/WR. c) represents the distribution of SST anomalies regressed onto the EA/WR.

562  
563  
564  
565  
566  
567  
568  
569  
570  
571  
572  
573  
574  
575  
576  
577  
578  
579  
580  
581  
582  
583  
584  
585  
586  
587  
588  
589  
590  
591  
592  
593  
594  
595  
596

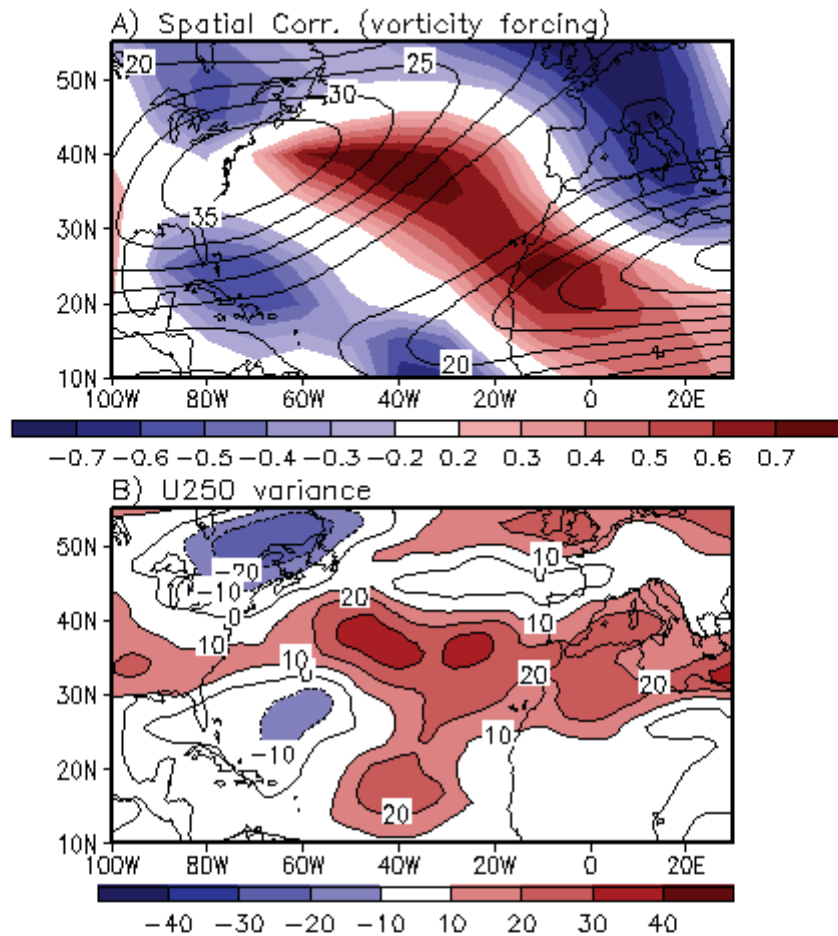


**Figure 5.** a) Same as Figure 4a except that transient eddy forcings of vorticities are given, respectively, at the grid points with 5-degree longitude-latitude interval over the Atlantic. Correlation values are plotted on the grid points where the transient eddy forcing of vorticity is given for generating the stationary wave in the model. Contours in a) denote the climatological upper-level (300hPa) westerlies. b) represents the distribution of upper-level (250hPa) zonal wind variance regressed onto the EA/WR.

597  
598  
599  
600  
601  
602  
603  
604  
605  
606  
607  
608  
609  
610  
611  
612  
613  
614  
615  
616  
617  
618  
619  
620  
621

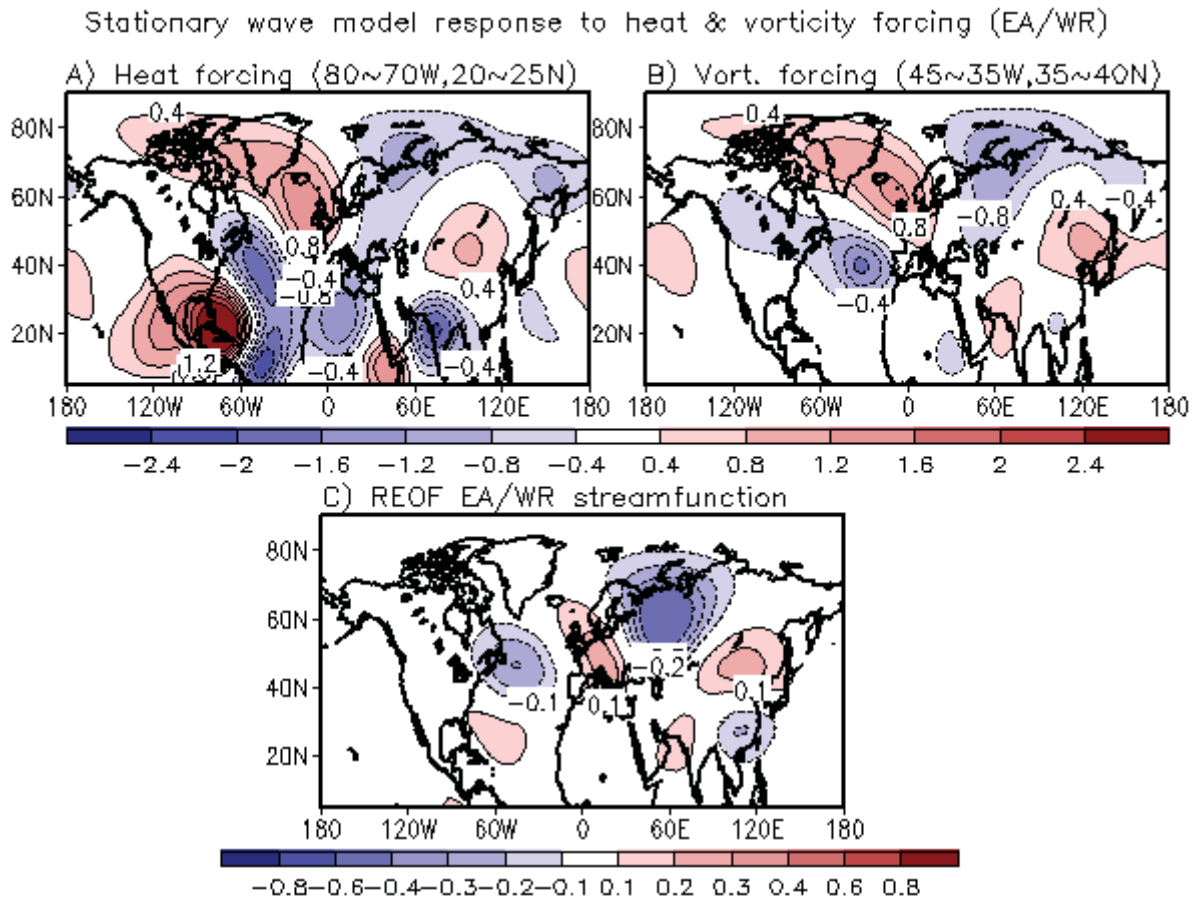


**Figure 6.** Upper panel: Streamfunction (divided by  $10^6$ ) of the simulated large-scale stationary wave propagation (a and b) similar to EA/WR pattern. a) represents the wave propagation forced by diabatic heat source, while b) by transient vorticity forcing. Geographical location of the forcing given in the model is 80~70°W, 25~25°N for the diabatic heat forcing, and 45~35°W, 35~40°N for the transient vorticity forcing, respectively. The 3-dimensional basic state in the SWM is the MERRA climatology computed from the past 33 winters (1979/80-2011/12). Lower panel: Observational teleconnection patterns for c) EA/WR obtained from REOF.

622  
623  
624  
625  
626  
627  
628  
629  
630  
631  
632  
633  
634  
635  
636  
637  
638  
639  
640  
641  
642  
643

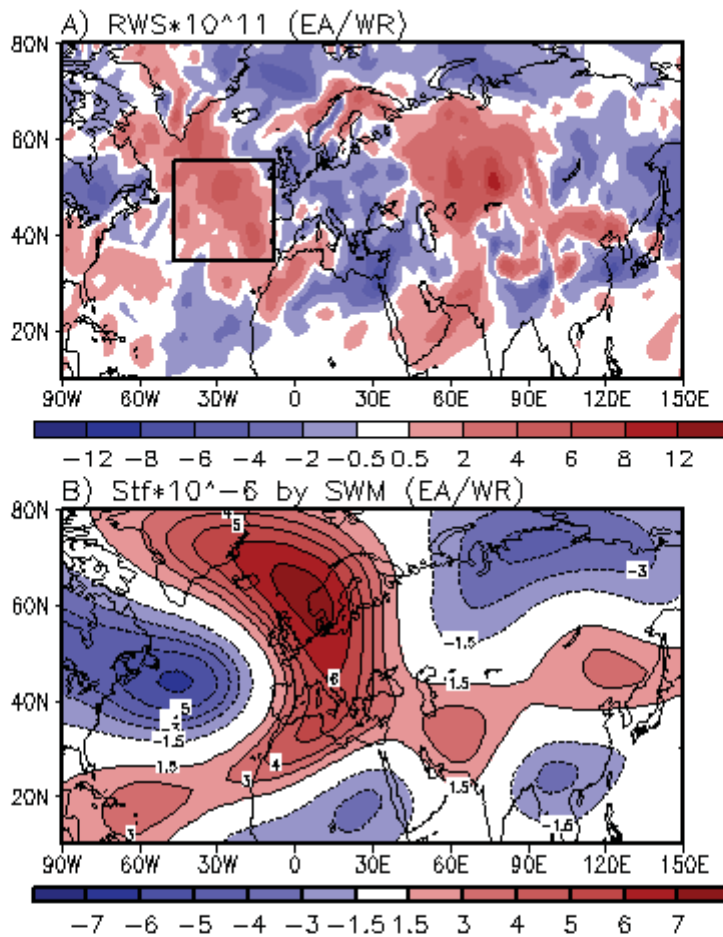


**Figure 7.** Upper panel: Rossby wave source (RWS) distribution of the observational large-scale stationary wave associated with EA/WR pattern. Source region is represented by positive values (red shading). Lower panel: The EA/WR-like teleconnection patterns reproduced by stationary wave model with the given RWS in the boxed regions shown in upper-panel. Boxed region is where magnitudes of spatial correlations found in Figure 5a are predominantly high.

644  
645  
646  
647  
648  
649  
650  
651  
652  
653  
654  
655  
656  
657  
658  
659  
660  
661  
662  
663

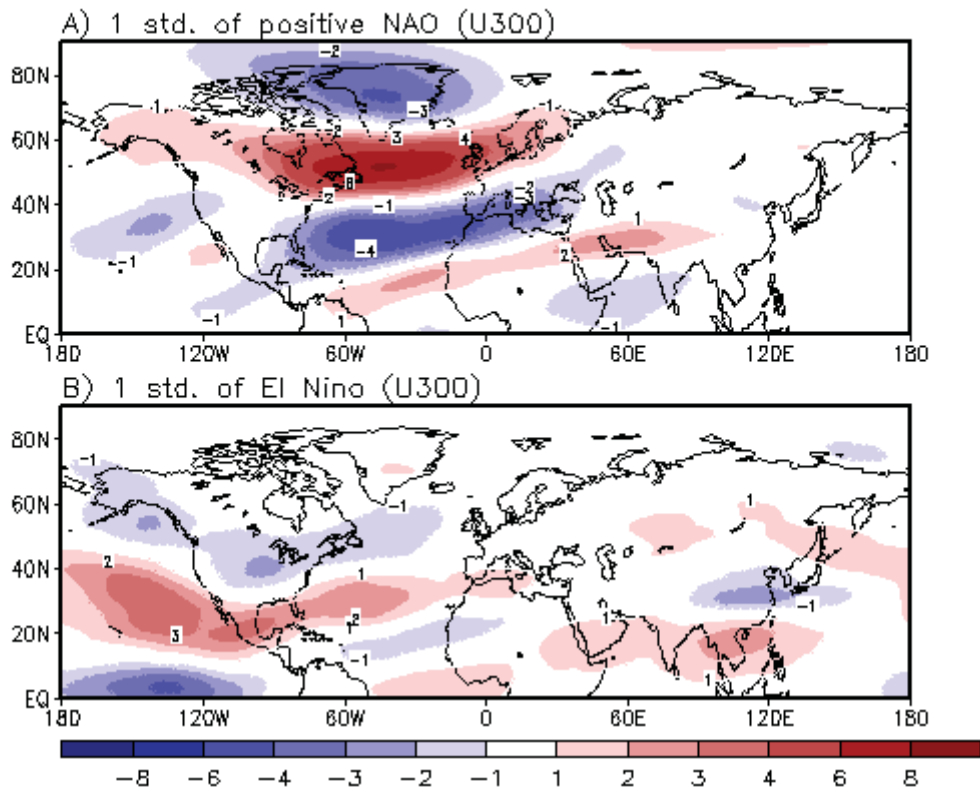


**Figure 8.** Upper panel (a): Distribution of one standard deviation of the positive NAO component in terms of upper-level (300hPa) westerly. Note that the climatology is the average of the upper-level westerlies over 1979/80-2011/12 DJF period. Lower panel (b): Same as a) but for the positive ENSO (i.e., El Niño) component

664  
665  
666  
667  
668  
669  
670  
671  
672  
673  
674  
675  
676  
677  
678  
679  
680  
681  
682  
683  
684

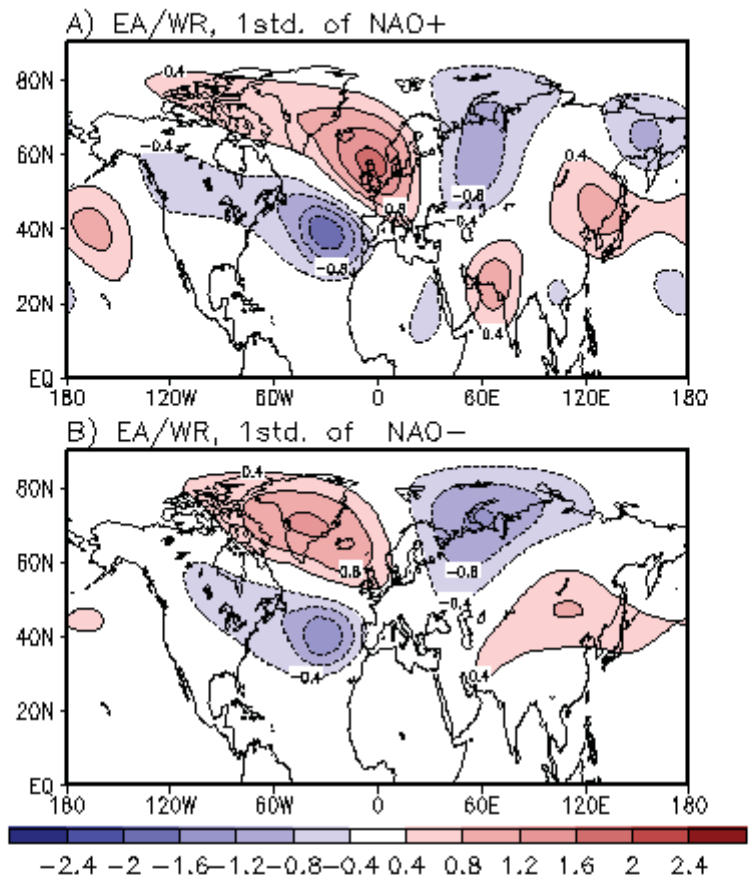


**Figure 9.** Simulated EA/WR-like Rossby wave train embedded in the modified climatological basis state where one standard deviation of a) positive NAO is added and b) negative NAO is added. Wave propagation patterns are plotted in terms of streamfunction (divided by  $10^6$ ).